IJHSR

ijhighschoolresearch.org

RESEARCH ARTICLE

Thermal Treatment of Disposable Beverage Bottles and Agricultural Mulching Film Mixture as a Chemical Recycling Approach

Eugene Ahn

Seoul International School, 15 Seongnam-daero, 1518 beon-gil, Sujeong-gu, Seongnam, Gyeonggi, 13113, Republic of Korea; eugeneahn0720@gmail.com

ABSTRACT: Biodegradable plastics are considered sustainable substitutes for conventional polymers, but their degradation requires controlled composting and is limited under natural conditions. In mixed waste streams, they also disrupt recycling processes and reduce the quality of recycled materials. This study investigates the thermal treatment of a disposable beverage bottle (DBB)–agricultural mulching film (AMF) mixture. The process reduced the decomposition temperature of DBB from 500 °C to 470 °C and shifted product distribution. Gas analysis revealed ethylene and other hydrocarbons of industrial relevance. The oil fraction contained a high proportion of organic acids, which can serve as chemical feedstocks. The solid product derived from the DBB–AMF mixture displayed improved crystallinity and stability compared with single pyrolysis. Raman spectroscopy showed a lower $I_{D/G}$ ratio (0.7), indicating fewer lattice defects. X-ray photoelectron spectroscopy, together with Brunauer–Emmett–Teller analysis, confirmed surface oxidation, bonding with metallic elements, and a high surface area (>300 m^2/g). These properties suggest high adsorption capacity and catalytic potential. Consequently, pyrolysis of the DBB–AMF mixture offers a practical approach to mixed plastic waste. The combination of textural order, accessible porosity, and surface functionality indicates potential for adsorption and catalytic applications, providing a practical route to valorize mixed plastic waste without strict feedstock segregation.

KEYWORDS: Environmental Engineering, Recycling, Waste Management, Polymers, Mixed Plastics.

Introduction

Disposable beverage bottle (DBB) is one of the most widely used non-biodegradable plastics, and agricultural mulching film (AMF) is a representative biodegradable plastic. Reducing plastic use is important, but on its own, it is not enough. We need new ways to treat waste that not only limit damage but also create value. Biodegradable plastics were developed as one possible solution. Agricultural mulching films are designed to decompose under certain conditions, and the market for such biodegradable materials has been growing rapidly. However, the benefits of using biodegradable materials are still limited. In ordinary soil or water, these plastics can last for years, and when they do degrade, they may release acidic byproducts. In other words, they are not a complete answer to the plastic waste problem.[1]

Chemical recycling by thermal treatment (e.g., pyrolysis) can treat mixed polymers and recover gases, oils, and solid carbon residue. Co-processing distinct polymers can also alter reaction pathways, reduce energy demand, and shift product distributions. Over their full life cycle, plastics are estimated to account for about 4.5% of global greenhouse gas emissions, with production alone responsible for nearly 15% of industrial carbon output, as shown in Figure 1.[1-3] The persistence of plastic debris in the environment is no longer a distant concern—it is an urgent problem linked to biodiversity loss and health risks such as cancer and neurological disease.

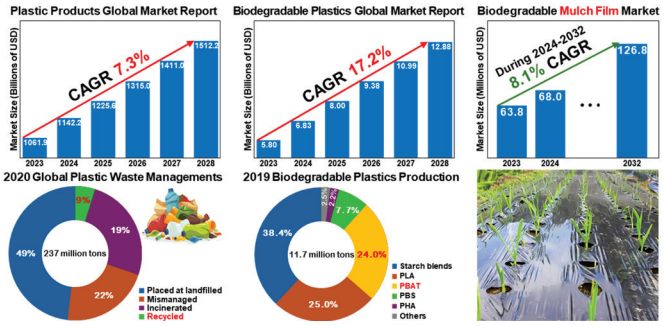

Figure 1: Global plastic products market report 2024 (left),[1] biodegradable plastics market report 2024 (center),[2] and projected market size of agricultural mulch films 2023–2032 (right).[3] Global plastics and biodegradable plastics markets continue to grow, with biodegradable plastics showing a much higher growth rate than conventional plastics. Despite this trend, inefficient waste management and environmental burdens persist, underscoring the need for effective chemical recycling of mixed plastic streams.

Recycling mixed plastics brings its own challenges. Biodegradable and conventional plastics look so similar that separating them is difficult. For instance, even a small amount of agricultural mulching film in disposable beverage bottles can weaken the material and reduce its clarity, thereby making their proper recycling impossible.[4] As a result, both kinds often end up in landfills or incinerators. This undermines many of the advantages of biodegradable plastics and shows the need for recycling methods that can handle mixed waste. Chemical recycling is one way forward. Among these methods, pyrolysis—heating plastics without oxygen—has received particular

DOI: 10.36838/IJHSR816.57

attention. The process produces gas, oil, and a solid residue. Gases like ethylene and hydrogen can be used as chemical feedstocks, and oils can be refined into acids and aromatics. Solid residue, however, has usually been dismissed as waste. Recent studies suggest otherwise: with the right properties, it can work as an adsorbent, a catalyst, or even as an electrode material.[5]

In this study, we examined the pyrolysis of a DBB/AMF mixture, where two plastics are processed together as shown in Figure 2. Avoid redundancy with temperature-sweep studies: all results are presented for a single operating point (500 °C, N_2, 1 min). Our focus was on DBB, a non-biodegradable plastic, and AMF, a biodegradable plastic often used in mulch films. We asked a simple question: can their interaction make recycling more efficient and produce solid residue with real value? To find out, we analyzed the solid product using Raman spectroscopy, X-ray photoelectron spectroscopy (XPS), and Brunauer–Emmett–Teller (BET) analysis. What we found was encouraging. The solid residue from AMF–DBB mixtures showed higher crystallinity, surface oxidation, and greater surface area than that from either plastic alone. These features are not just technical details; they mean the material may have potential for adsorption or catalytic applications, instead of being thrown away. This study shows that co-pyrolysis of DBB and AMF produces a solid residue with improved structure and surface properties compared to single plastics. It demonstrates that mixed plastic waste can be directly converted into functional carbon materials for adsorption or catalysis.

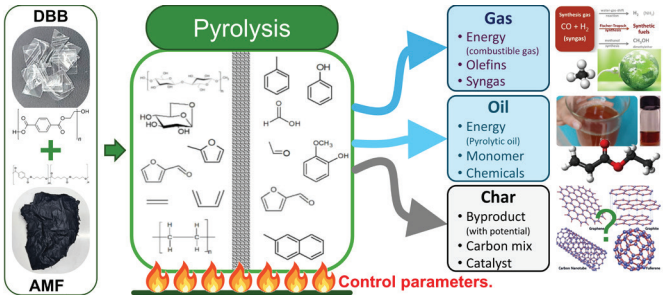

Figure 2: Schematic illustration of the pyrolysis of the DBB-AMF mixture under controlled parameters. The interaction between biodegradable AMF and non-biodegradable DBB promotes the formation of a solid residue with enhanced crystallinity and surface area, indicating potential value beyond simple waste disposal.

Methods

Materials and Pyrolysis:

A physical mixture of commercially available AMF (made mainly from polybutylene adipate terephthalate) and DBB (used water bottles made from polyethylene terephthalate) was used as feedstock. The thermal treatment procedure of the DBB–AMF mixture is depicted in Figure 3.

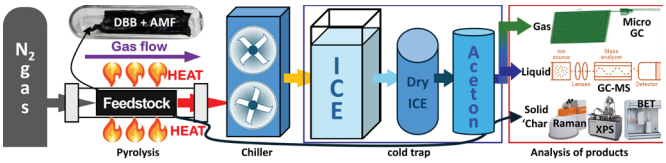

Figure 3: Schematic illustration of the experimental setup for the pyrolysis of the DBB–AMF mixture and subsequent product analyses. The system enables controlled thermal treatment and subsequent separation and analysis of gas, liquid, and solid products for comparative evaluation.

The thermal treatment was carried out between 100 and 900 °C (10 °C/min) in a nitrogen atmosphere. AMF and DBB were physically mixed in equal weight proportions (1 g total). To provide reference data, single-component runs of AMF and DBB (0.5 each) were also conducted. All feedstocks were purged with ultra-high-purity nitrogen (99.9%) for 10 min to eliminate residual oxygen. Preliminary thermal analysis over 100–900 °C identified 450–500 °C as the main decomposition range; therefore, subsequent co-pyrolysis experiments were performed at 500 °C based on the identified decomposition range. A continuous nitrogen flow of 100 mL/min was maintained during pyrolysis, which was performed at 500 °C with a heating rate of 10 °C/min. The target temperature was maintained for 1 min before cooling. Product yield was calculated according to:

$$\textit{Yield}\ (wt.\%) = \frac{\textit{Mass of pyrolyzate}\ (mg)}{\textit{Mass of feedstock}\ (mg)} \times 100(\%)$$

Analysis:

Non-Condensable Gases:

Non-condensable gases were analyzed using a micro gas chromatograph (GC) connected directly to the outlet (Figure 3). Gas composition was quantified under the conditions listed in Table 1. Module A ramped from 50 to 100 °C in 50 s, while Module B ramped from 50 to 110 °C in 60 s. Each module was then held for 40 s, giving a total run time of 130 s.

Table 1: Instrument setting for micro-GC analysis. The temperature programs for Modules A and B were optimized to ensure reliable separation and quantification within a total analysis of 130 s.

Model	Conditions	Column	Column setting					
			Carrier	Column P	Initial T	Ramping t	Final T	Analysis t
INFICON Analyzer	Module A	Rt- 5A	Ar	20 psi	50°C-40s	50 s	100°C-40s	130s
	Module B	Rt-Q-B	He	17 psi	50°C-30s	60 s	110°C-40s	130s

Condensable Products:

Condensable fractions were collected using an ice-cooled condenser and subsequently analyzed with a GC–MS system (Agilent 8890 GC–5977B). The operating parameters are provided in Table 2. The temperature was programmed from 40 to 280 °C at 10 °C/min.

Table 2: Instrument setting for the GC–MS analysis. The program was designed to enable separation of volatile and semi-volatile compounds up to 280 °C within a total run time of 45 min.

Column	Column setting			
	Initial t	Ramping	Final t	Total time
HP-5MS	40°C-240s	10 °C/min	280°C-900s	45 min

Solid Product:

The solid residues were examined by X-ray fluorescence (XRF), Brunauer–Emmett–Teller (BET) surface analysis, Raman spectroscopy, and X-ray photoelectron spectroscopy (XPS). Raman spectra (inVia, Renishaw, UK) were obtained using a 532 nm laser in the 1200–3200 cm^{-1} range. XPS (NEXSA, Thermo Fisher, USA) was used to identify bonding states, including C–C, C=C, C–O, and C=O, with a spot size of 400 μm. BET measurements (ASAP 2020, Micromeritics, USA) were conducted after degassing the samples at 300 °C for 120 min, with adsorption data collected over P/P_0 = 0.01–

0.995. Bulk elemental composition was determined by XRF (ZSX Primus, Rigaku, Japan). By combining these techniques, we were able to capture complementary information: Raman provided insight into graphitic order and defect density, XPS revealed surface chemistry, BET quantified porosity and surface area, and XRF confirmed elemental composition.

Results and Discussion

All Products after Co-Pyrolysis:

Figure 4 shows the mass balance of products, expressed as yield (wt.%), from the pyrolysis of DBB, AMF, and their mixture. During pyrolysis of the mixture, volatile intermediates formed and condensed on the reactor walls as wax (C > 20 oxo-carbon species). This wax subsequently degraded into liquid products containing oxygenated compounds with carbon numbers over 20, which could further crack into light gases such as CO_2, H_2, CO, and C_1–C_4 hydrocarbons. The volatile fraction was not quantified due to experimental limitations. Therefore, the pyrolysis of the mixture produced higher yields of gas and solid product compared to the single pyrolysis of either DBB or AMF. In contrast, the oil yield from the mixture was lower than that obtained from individual polymers. The yield of wax during pyrolysis of the mixture was greater than that from AMF alone but less than that from DBB.[6]

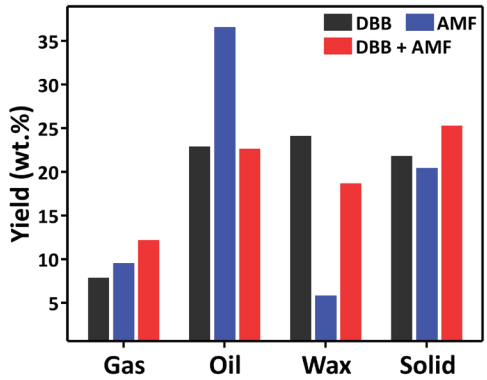

Figure 4: Comparison of product yields achieved by pyrolysis of DBB, AMF, and DBB–AMF mixture. Co-pyrolysis of the DBB–AMF mixture produced higher gas and solid yields and a lower oil yield than single-component pyrolysis. This behavior reflects changes in reaction pathways caused by interactions between the two polymers.

Thermo-Reaction Results:

When DBB and AMF were pyrolyzed together, the profile shifted. The maximum decomposition temperature was observed at 472 °C, lower than pure DBB but higher than pure AMF. This intermediate position suggests that the two polymers interact during pyrolysis. AMF likely generates radicals or fragments that accelerate chain scission in DBB, while DBB appears to stabilize AMF slightly, delaying its breakdown compared with the neat film. These results show that DBB and AMF do not simply degrade in parallel. Their interaction creates a modified decomposition pathway that lowers the energy requirement relative to DBB alone. The shift in thermal behavior also points to potential changes in product distribution, which is important when considering the efficiency and outcomes of co-pyrolysis for mixed plastic systems. Such interactions are commonly attributed to hydrogen abstraction and radical transfer between polymer fragments, which can promote chain scission in more stable polymers such as PET.[7] Similar co-pyrolysis behavior has been reported in mixed polymer systems, where reactive intermediates generated from one component modify the decomposition pathway of another polymer.[8]

Non-Condensable Products:

Table 3 summarizes the composition of non-condensable gases generated during the pyrolysis of DBB, AMF, and their mixture. The results reveal clear differences among the three cases, reflecting the effect of polymer interactions during the pyrolysis of the mixture. The major gaseous products were H_2, CO, CO_2, CH_4, and light hydrocarbons including C_2H_4, C_2H_6 C_3H_6, and C_3H_8. These gases are of considerable industrial importance. Hydrogen and methane can serve as fuels or as feedstocks for ammonia synthesis. CO, when combined with H2, produces syngas, which is widely used in chemical conversion processes. Although CO_2 is a greenhouse gas, it also has established applications in methanol synthesis, plastics manufacturing, and carbon capture and utilization technologies. Light olefins and paraffins (C_2–C_3 hydrocarbons) are critical raw materials for polymer production and other chemical syntheses.

Table 3: Non-condensable gases are released from the pyrolysis of DBB, AMF, and the DBB–AMF mixture. Co-pyrolysis alters the relative distribution of major gaseous products, indicating the influence of polymer interactions on gas formation pathways.

Product	H_2	CO	CH_4	CO_2	C_2H_4	C_2H_6	C_3H_6	C_3H_8
DBB	< 3%	> 10%	3 - 10%	3 - 10%	3 - 10%	< 3%	3 - 10%	< 3%
AMF	< 3%	3 - 10%	< 3%	> 10%	< 3%	< 3%	< 3%	< 3%
DBB+AMF	< 3%	3 - 10%	< 3%	> 10%	3 - 10%	< 3%	< 3%	< 3%

The relative yields of these gases are sensitive to process parameters such as temperature, catalyst, and atmosphere. Proper control of these conditions can enhance both the selectivity and economic value of non-condensable products obtained from the pyrolysis of a mixture.[9]

Condensable Products:

Table 4 lists the condensable products (oils) obtained from the pyrolysis of DBB, AMF, and their mixture. The main components included acids, phenyls, adipates, phthalates, and polycyclic aromatic hydrocarbons (PAHs). Among these, acids represented the dominant fraction, emphasizing their importance as recyclable feedstocks for industrial use. Their prevalence demonstrates both the environmental and economic potential of the pyrolysis process.

Table 4: Condensable compounds formed from the pyrolysis of DBB, AMF, and the DBB–AMF mixture. Co-pyrolysis modifies the distribution of oxygenated and aromatic compounds, indicating that feedstock interactions influence oil composition and potential reuse.

Product	Adipates	Phthalates	Phenyls	Acids	PAHs
DBB	~0%	< 3%	< 3%	> 10%	< 3%
AMF	3 - 10%	3 - 10%	< 3%	> 10%	~0%
DBB+AMF	3 - 10%	3 - 10%	< 3%	> 10%	< 3%

DOI: 10.36838/IJHSR816.57

As with non-condensable gases, the distribution of condensable compounds was influenced by process parameters such as temperature, catalyst, and residence time. Notably, the interaction between AMF-derived volatiles and DBB intermediates suppressed terephthalic acid formation while favoring the production of adipic acid derivatives.[10] Feedstock composition also had a marked effect: AMF alone, DBB alone, and AMF–DBB mixtures produced distinct chemical profiles. This variation highlights the role of feedstock selection in tailoring oil yields and composition for targeted applications.[s]

Solid Product:

The solid product derived from the DBB and AMF pyrolysis is a carbon-rich residue that remains after the volatilization of organic species during pyrolysis. Although often regarded as a byproduct, in this study, the pyrolysis parameters were adjusted to improve its structure and functionality. The solid product exhibited structural features associated with potential applications in catalyst, adsorbent, or electrode material, emphasizing its importance as a reusable carbon resource.

Compositional Impurities:

X-ray fluorescence (XRF) analysis identified differences in composition among the solid products obtained from DBB, AMF, and their mixtures (Table 5). DBB-derived solid product was almost entirely carbon (>99.9 wt.%), showing negligible inorganic residue. In contrast, AMF-derived solid product contained a higher fraction of inorganics, primarily Ca, Si, and Mg. These elements are consistent with common AMF additives such as magnesium oxide pigments, calcium carbonate fillers, and silicate-based processing aids. In mixture pyrolysis systems, the overall inorganic fraction decreased gradually, although Ca, Si, and Mg remained detectable. Their persistence reflects the volatilization of the organic matrix and the concentration of thermally stable mineral phases. After co-pyrolyzed DBB–AMF solid product, decomposition of carbonates produced refractory oxides, accounting for the retention of Mg- and Si-bearing phases.[12]

Table 5: XRF results of the solid products derived from pyrolysis of DBB, AMF, and DBB–AMF mixture under different conditions. The presence of these thermally stable inorganic species in the DBB–AMF solid indicates selective retention of mineral phases within the carbon framework during co-pyrolysis.

Composition (wt.%)	C	Ca	Si	Mg
DBB	99.911	0.034	0.041	0.014
AMF	98.012	1.102	0.582	0.696
DBB+AMF	99.142	0.506	0.251	0.101

At 500 °C, the solid product from DBB–AMF mixtures showed the highest Ca and Mg contents. The presence of finely dispersed oxides at this stage may help stabilize the carbon framework, maintaining pore architecture during matrix shrinkage. As a result, the DBB–AMF mixture-derived solid product combines graphitic carbon with stable oxide phases and a tunable micro–mesoporous structure. These features highlight their potential as multifunctional carbon materials for applications such as ultrafine particle adsorption, hybrid electrode, catalysis, and lubricants.[13]

Specific Surface Area:

Figure 5 summarizes the surface area analyses of the solid products obtained from DBB, AMF, and their mixtures. Adsorption–desorption isotherms were used to determine specific surface area, pore size distribution, and the presence of micro-, meso-, and macropores. The measurements provided direct insight into the pore architecture and adsorption capacity of each sample. The DBB-derived solid product exhibited a relatively high surface area of ~420 m^2/g with an average pore size of 2.5 nm. Its BET constant was 241, and the corresponding hysteresis loop confirmed the coexistence of both micropores (<2 nm) and mesopores (2–50 nm). In contrast, AMF-derived solid product displayed much poorer textural properties, with a specific surface area of only 57.7 m^2/g and an average pore size of 16.1 nm. Its BET constant was also low (28.6), and the isotherm showed only minimal evidence of mesoporosity, reflecting a less developed pore network. The mixed DBB–AMF-derived solid product presented markedly different behavior. It showed a high specific surface area of ~330 m^2/g, an average pore size of 2.3 nm, and the highest BET constant among the three systems (496.6).

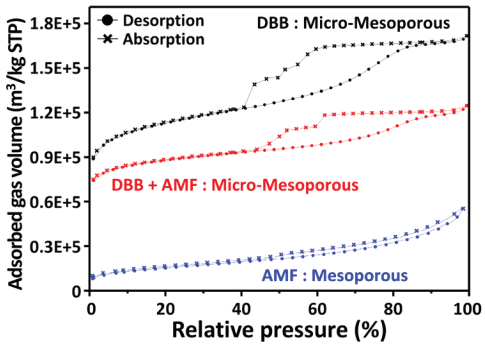

Figure 5: BET analysis of solid product derived by pyrolysis of DBB, AMF, and DBB–AMF mixture. The DBB–AMF-derived solid exhibits a combined micro–mesoporous structure with a high BET constant, indicating enhanced adsorption interactions compared to the single-component solids. This micro–mesoporous architecture reflects modification of pore structure through co-pyrolysis rather than a simple averaging of the two precursors.

The corresponding isotherm and hysteresis loop revealed a well-developed pore structure with abundant micropores and mesopores. The much larger BET constant suggests stronger adsorption interactions between the solid product's surface and nitrogen molecules, indicative of improved surface energetics. Comparing the three conditions, the DBB/AMF mixture clearly produced a solid carbon with improved textural properties relevant to functional applications. Although its surface area was slightly lower than that of the DBB-derived solid product, the significantly higher BET constant and the abundance of micropores point to superior adsorption potential. The dispersion of micropores within a relatively stable mesoporous framework likely provided additional accessible sites, leading to enhanced capacity for adsorptive and catalytic processes.[14]

These results highlight that pyrolysis of DBB–AMF mixture modifies the pore architecture as micro-mesoporous (i.e.,

type IV isotherm) in a favorable manner, rather than a simple average of the two precursors, the DBB–AMF-derived solid product combined features of both systems—retaining high surface area, improving pore size uniformity, and strengthening adsorption interactions. This outcome demonstrates that pyrolysis of a mixture can be strategically used to tailor the textural properties of the solid products, producing materials with enhanced potential for applications such as adsorption, catalysis, and possibly energy storage electrodes.[15]

Atomic Bonding:

Raman spectroscopy was used to evaluate the bonding states and structural order of solid products, as shown in Figure 6. The analysis focused on the D band (~1350 /cm), G band (~1580 /cm), and 2D band (~2700 /cm), which provide information on defect density, sp^2 carbon bonding, and graphene layer stacking, respectively. The D band originates from lattice imperfections, while the G band reflects the degree of sp^2 hybridization. The 2D band is associated with graphitic stacking, with higher intensity and narrower width indicating fewer layers.[16] The structural quality of the solid products was assessed using the $I_{D/G}$ and $I_{2D/G}$ ratios. DBB-derived solid product exhibited an $I_{D/G}$ ratio of 0.84 and $I_{2D/G}$ of 0.18. AMF-derived solid product showed an ID/G of 0.87 and an $I_{2D/G}$ of 0.92, while the DBB–AMF mixture-derived one had the lowest $I_{D/G}$ (0.73) and an intermediate $I_{2D/G}$ (0.37).

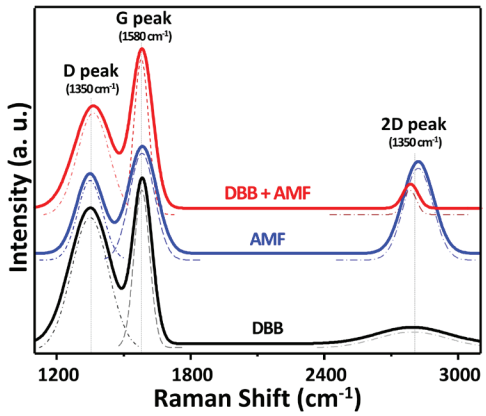

Figure 6: Raman spectra of the solid product derived by pyrolysis of DBB, AMF, and DBB–AMF mixture. Lower $I_{D/G}$ ratios and intermediate I2D/G values observed for the mixed sample indicate increased graphitic ordering with partial layer development. This structural modification reflects carbon reorganization driven by interactions between DBB- and AMF-derived intermediates during co-pyrolysis.

Since lower $I_{D/G}$ ratios correspond to higher crystallinity, all solid products displayed partial graphitic ordering ($I_{D/G}$ < 1), with the DBB–AMF mixture-derived solid product showing the highest degree of order. With respect to layer structure, the AMF-derived solid product showed the highest $I_{2D/G}$ ratio, suggesting a closer approach to single-layer graphene. DBB-derived solid product exhibited the lowest ratio, consistent with multilayer stacking, while the DBB–AMF mixture-derived solid product displayed an intermediate value, indicating a partially layered structure. Raman results demonstrate that pyrolysis of DBB and AMF mixture enhances the solid product's crystallinity beyond that of the individual polymers. The mixture-derived solid product combines improved graphitic ordering with a moderate layered structure, confirming that thermochemical interactions between DBB and AMF during pyrolysis of the mixture yield carbon with superior structural characteristics.[17]

Chemical Reactive Sites:

X-ray photoelectron spectroscopy (XPS) was used to examine the surface composition and bonding states of DBB- and AMF-derived solid products (Figure 7(a-b)). DBB-derived solid product displayed a clean spectrum dominated by the C_{1s} signal, with only a small O_{1s} contribution. Quantitatively, the composition was 85.8% carbon and 13.9% oxygen, confirming the high purity already suggested by its sharp Raman G band and the absence of inorganic residues in the XRF results. High-resolution spectra identified a strong sp^2 C=C peak at 284.6 eV, while signals from C–O and C=O were minimal, indicating a well-ordered carbon matrix with limited oxidation. AMF-derived solid product, in contrast, exhibited a much higher oxygen fraction (47.7%) and a significantly reduced carbon content (37.1%). Impurity peaks for Si, Ca, and Mg were also present, consistent with the use of $CaCO_3$, MgO, and silicate additives in AMF films. Its high-resolution spectra showed strong C=C bonding but also broad C–O and C=O features, suggesting partial oxidation and a more heterogeneous surface chemistry than DBB.[18]

The DBB–AMF mixture produced the solid product with intermediate characteristics presented in Figure 7(c). The survey spectra revealed 40.4% carbon, 43.5% oxygen, and 16.1% impurities, with clear signals from Ca, Si, and Mg. High-resolution analysis confirmed the presence of C=C, C=O, and C–Si bonds, reflecting a surface that combined graphitic domains with metallic oxide associations. Compared with single polymers, the mixture-derived solid product maintained a reasonable sp^2 carbon fraction while incorporating stable oxides into the structure. This hybrid character suggests that thermochemical interactions between DBB and AMF promote both carbon ordering and the retention of inorganic species on the surface, features not observed to the same extent in the individual solid product.[19]

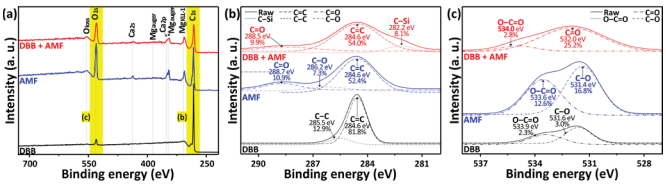

Figure 7: (a) XPS spectra of the solid products derived from pyrolysis of DBB, AMF, and DBB–AMF mixture; (b, c) magnified views of (a). Distinct differences in carbon–oxygen bonding and impurity signals indicate that the mixed sample exhibits intermediate surface chemistry, combining sp2 carbon domains with Ca-, Si-, and Mg-associated species. This hybrid surface structure reflects thermochemical interactions during co-pyrolysis and differentiates the DBB–AMF-derived solid from those produced by single polymers.

When integrated with the Raman, BET, and XRF results, the XPS data provide a comprehensive view of the solid product's structure. Raman analysis demonstrated that the DBB–AMF-derived solid product had the lowest $I_{D/G}$ ratio,

DOI: 10.36838/IJHSR816.57

indicative of superior crystallinity, while BET measurements showed high surface area and strong adsorption potential. XRF confirmed the persistence of Ca, Si, and Mg across pyrolysis temperatures, which aligns with the impurity signals detected in XPS. Taken together, these results indicate that pyrolysis of the mixture yields a hybrid carbon–oxide material with enhanced graphitic order, accessible porosity, and surface functionalization. Such a combination of properties distinguishes the DBB–AMF-derived solid product from single-polymer ones and supports its potential for catalytic and adsorption applications.

■ Conclusion

This study investigated the pyrolysis of DBB and AMF mixture to address mixed plastic waste while evaluating the potential of solid residue as a functional carbon material. Pyrolysis of the mixture modified the thermal decomposition pathway, reduced the degradation temperature, and enhanced the quality of gaseous, liquid, and solid products.

- The maximum degradation temperature of the DBB–AMF mixture was reduced to 472 °C, confirming thermochemical interactions and improved energy efficiency.
- Gas products contain hydrogen, methane, CO, CO_2, and light hydrocarbons; oil fractions were enriched in acidic compounds suitable for chemical feedstocks.
- XRF analysis showed the presence of Ca, Si, and Mg in the solid products, and BET results demonstrated high surface area, meso-micropores, and a high BET constant, indicating strong adsorption performance.
- Raman spectroscopy revealed the lowest $I_{D/G}$ ratio (0.73) for DBB–AMF-derived solid product, signifying superior crystallinity; XPS confirmed sp^2 C=C bonding, evidencing partial oxidation and oxide dispersion.

■ Acknowledgments

The author would like to express his sincere gratitude to Professor Jaechan Lee at Sungkyunkwan University, Republic of Korea, for allowing him to conduct the experiments and helping him with the analysis throughout this research, as well as his mentorship with valuable guidance.

■ References

1. Emadian, S. M.; Onay, T. T.; Demirel, B. Biodegradation of bioplastics in natural environments. *Waste Manag*. **2017**, 59, 526–536. https://doi.org/10.1016/j.wasman.2016.10.006
2. Park, Y. K.; Lee, J. Achievements in the Production of Bioplastics from Microalgae. *Phytochem. Rev*. **2023**, *22*, 1147–1165. https://doi.org/10.1007/s11101-021-09788-8
3. The Business Research Company. *Plastic Products Global Market Report 2025*; The Business Research Company: London, UK, **2025**. Available online (accessed July 2025): https://www.thebusinessresearchcompany.com/report/plastic-products-global-market-report.
4. Fortune Business Insights. *Biodegradable Mulch Film Market Size, Share & Industry Analysis*; **2024**. Available online (accessed July 2025): https://www.fortunebusinessinsights.com/biodegradable-mulch-film-market-102759.
5. Czajczyńska, D.; Anguilano, L.; Ghazal, H.; Krzyżyńska, R.; Reynolds, A. J.; Jouhara, H. Potential of Pyrolysis Processes in the Waste Management Sector. *Therm. Sci. Eng. Prog*. **2017**, *3*, 171–197. https://doi.org/10.1016/j.tsep.2017.06.003
6. Frederick, W. J.; Hupa, M.; Uusikartano, T. Volatiles and Char Carbon Yields during Black Liquor Pyrolysis. *Bioresour. Technol.* **1994**, *48* (1), 59–64. https://doi.org/10.1016/0960-8524(94)90137-6
7. Xing, B.; Hu, Y.; Wang, S. Study of synergistic effects in co-pyrolysis of biomass and plastics from the perspective of phase reactions. *J. Anal. Appl. Pyrolysis.* **2025**, 186, 106951. https://doi.org/10.1016/j.jaap.2025.106951
8. Nardella, F.; Bellavia, S.; Mattonai, M.; Ribechini, E. Co-pyrolysis of biomass and plastic: Synergistic effects and estimation of elemental composition of pyrolysis oil by analytical pyrolysis–gas chromatography/mass spectrometry. *Bioresour. Technol*. **2022**, *354*, 127170. https://doi.org/10.1016/j.biortech.2022.127170
9. Aldas, M.; Pavon, C.; de la Rosa-Ramírez, H.; Ferri, J. M.; Bertomeu, D.; Samper, M. D.; López-Martínez, J. The Impact of Biodegradable Plastics in the Properties of Recycled Polyethylene Terephthalate. *J. Polym. Environ*. **2021**, *29* (8), 2686–2700. https://doi.org/10.1007/s10924-021-02073-x
10. Abnisa, F.; Daud, W. M. A. W. A Review on Co-Pyrolysis of Biomass: An Optional Technique to Obtain a High-Grade Pyrolysis Oil. *Energy Convers. Manag*. **2014**, *87*, 71–85. https://doi.org/10.1016/j.enconman.2014.07.007
11. Z. Hu, L. Tang, P. Gao, B. Wang, C. Zhang, Y. Sheng, W. Pan, L. Ding, X. Chen, F. Wang. Elucidating synergistic effects during co-pyrolysis of plastics and paper in municipal solid waste: thermal behavior and product characteristics. *Bioresour. Technol*. **2025**, 416, 131831. https://doi.org/10.1016/j.biortech.2024.131831
12. Di Blasi, C. Modeling chemical and physical processes of wood and biomass pyrolysis. *Prog. Energy Combust. Sci.* **2008**, *34* (1), 47–90. https://doi.org/10.1016/j.pecs.2006.12.001
13. Yu, J.; Guo, Q.; Ding, L.; Gong, Y.; Yu, G. Study on the Effect of Inherent AAEM on Char Structure Evolution during Coal Pyrolysis by In-Situ Raman and TG. *Fuel* **2021**, *292*, 120406. https://doi.org/10.1016/j.fuel.2021.120406
14. Li, Z.; Deng, L.; Kinloch, I. A.; Young, R. J. Raman Spectroscopy of Carbon Materials and Their Composites: Graphene, Nanotubes and Fibres. *Prog. Mater. Sci.* **2023**, *135*, 101089. https://doi.org/10.1016/j.pmatsci.2023.101089
15. Al-Ghouti, M. A.; Da'ana, D. A. Guidelines for the Use and Interpretation of Adsorption Isotherm Models: A Review. J. Hazard. Mater. **2020**, 393, 122383. https://doi.org/10.1016/j.jhazmat.2020.122383
16. Yu, J.; Xia, W.; Areeprasert, C.; Ding, L.; Umeki, K.; Yu, G. Catalytic Effects of Inherent AAEM on Char Gasification: A Mechanism Study Using In-Situ Raman. *Energy* **2022**, *238* (C), 122074. https://doi.org/10.1016/j.energy.2021.122074
17. Yu, J.; Gua, Q.; Ding, L.; Gong, Y.; Yu, G. Studying Effects of Solid Structure Evolution on Gasification Reactivity of Coal Chars by In-Situ Raman Spectroscopy. *Fuel* **2020**, *270*, 117603. https://doi.org/10.1016/j.fuel.2020.117603
18. Huang, Y.; Liu, S.; Akhtar, M. A.; Li, B.; Zhou, J.; Zhang, S.; Zhang, H. Volatile–Char Interactions during Biomass Pyrolysis: Understanding the Potential Origin of Char Activity. *Bioresour. Technol.* **2020**, *316*, 123938. https://doi.org/10.1016/j.biortech.2020.123938
19. Ayiania, M.; Smith, M.; Hensley, A. J. R.; Scudiero, L.; McEwen, J.-S.; Garcia-Perez, M. Deconvoluting the XPS Spectra for Nitrogen-Doped Chars: An Analysis from First Principles. *Carbon* **2020**, *162*, 528–544. https://doi.org/10.1016/j.carbon.2020.02.065

Authors

Eugene Ahn is an 11th-grade student at Seoul International School, Republic of Korea. He is motivated by a strong interest in environmental issues, and he seeks to combine computer science with materials-based approaches, which inspired him to carry out this research project. He would like to pursue research in materials science, environmental engineering, and the application of artificial intelligence to these fields in the future.

DOI: 10.36838/IJHSR816.57